Electronic and optical properties of lead iodide

R. Ahuja, H. Arwin, A. Ferreira da Silva, C. Persson, J. M. Osorio-Guillén et al.

Citation: J. Appl. Phys. **92**, 7219 (2002); doi: 10.1063/1.1523145
View online: http://dx.doi.org/10.1063/1.1523145
View Table of Contents: http://jap.aip.org/resource/1/JAPIAU/v92/i12
Published by the American Institute of Physics.

Electronic and optical properties of lead iodide

R. Ahuja[a)]
Condensed Matter Theory Group, Department of Physics, Uppsala University, Box 530, SE-751 21 Uppsala, Sweden

H. Arwin
Department of Physics and Measurement Technology, Linköping University, SE-581 83 Linköping, Sweden

A. Ferreira da Silva
Instituto de Fisica, Universidade Federal da Bahia, Campus Universitario de Ondina 40 210 340 Salvador, Ba, Brazil

C. Persson, J. M. Osorio-Guillén, and J. Souza de Almeida
Condensed Matter Theory Group, Department of Physics, Uppsala University, Box 530, SE-751 21, Uppsala, Sweden

C. Moyses Araujo
Condensed Matter Theory Group, Department of Physics, Uppsala University, Box 530, SE-751 21, Uppsala, Sweden and Instituto de Fisica, Universidade Federal da Bahia, Campus Universitario de Ondina 40 210 340 Salvador, Ba, Brazil

E. Veje
Department of Electronic Power Engineering, Technical University of Denmark, Building 325, DK-2800 Lyngby, Denmark

N. Veissid and C. Y. An
Instituto Nacional de Pesquisas Espaciais, INPE/LAS–C.P. 515, 12 201 970 São José dos Campos, SP, Brazil

I. Pepe
Instituto de Fisica, Universidade Federal da Bahia, Campus Universitario de Ondina 40 210 340 Salvador, Ba, Brazil and LPCC–College de France, F-75231, Paris, France

B. Johansson
Condensed Matter Theory Group, Department of Physics, Uppsala University, Box 530, SE-751 21, Uppsala, Sweden

(Received 12 June 2002; accepted 27 September 2002)

The electronic properties and the optical absorption of lead iodide (PbI_2) have been investigated experimentally by means of optical absorption and spectroscopic ellipsometry, and theoretically by a full-potential linear muffin-tin-orbital method. PbI_2 has been recognized as a very promising detector material with a large technological applicability. Its band-gap energy as a function of temperature has also been measured by optical absorption. The temperature dependence has been fitted by two different relations, and a discussion of these fittings is given. © *2002 American Institute of Physics.* [DOI: 10.1063/1.1523145]

I. INTRODUCTION

Lead iodide (PbI_2) is a very important material with a technological applicability as a room-temperature radiation detector. It is a wide-band-gap semiconductor ($E_g > 2$ eV) with high environmental stability efficiency.[1–4] The performance of the detector cannot be fully understood unless its electronic and optical properties are determined. Recently, its band-gap energy and thermal properties were determined by photoacoustic spectroscopy.[4,5] A single crystal of PbI_2 was grown by the Bridgman method with the *c*-axis oriented perpendicular to the growth axis.[4]

The purpose of this work is to obtain the electronic structure of PbI_2, its dielectric functions ϵ_1 and ϵ_2 by ellipsometry and theoretically by full-potential linear muffin-tin-orbital (FPLMTO) method,[6] and the temperature dependence of the measured band-gap energy by optical absorption. The obtained $E_g(T)$ can be fitted by two different methods,[7,8] leading to E_g (0 K) and E_g (300 K).

II. EXPERIMENTAL DETAILS

A crystal of PbI_2 was grown by the Bridgman method with the *c*-axis oriented perpendicular to the growth axis.[4] The photoacoustic spectroscopy (PAS) result was extracted from Ref. 4. Additionally, from transmission (TR) data we have observed a broad spectrum spanning the wavelength interval, 850–360 nm corresponding to photon energies from 1.46 to 3.44 eV. The experimental apparatus is shown in our previous article by Ahuja *et al.*[9] The temperature dependence of the optical absorption (ABS) was measured by the following procedures.

The samples were mounted in a closed-cycle helium refrigeration system and studied at temperatures between 10

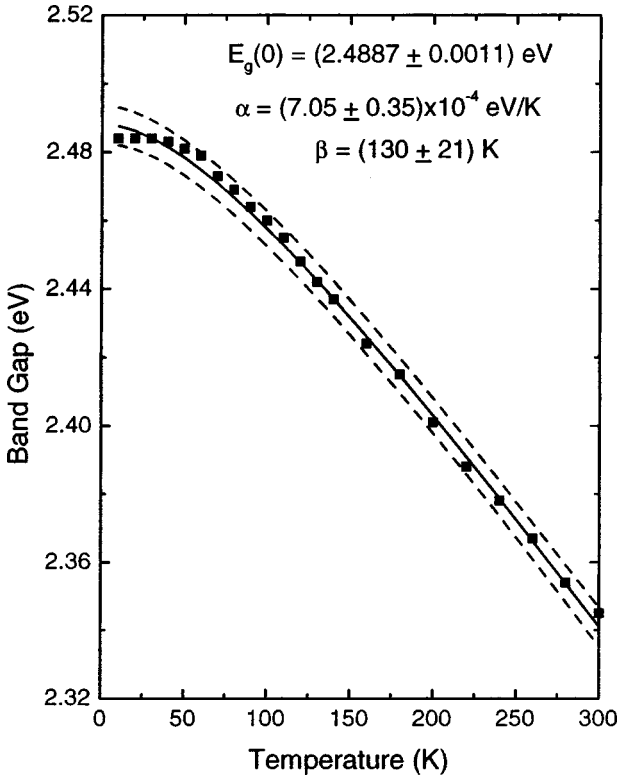

FIG. 1. Full squares are the experimentally determined values, with ABS measurements, for the band-gap energy of PbI_2 as a function of temperature. Curve shows the best fit to the experimental data obtained with the use of Eq. (3). Dashed points represent lower and upper error limits.

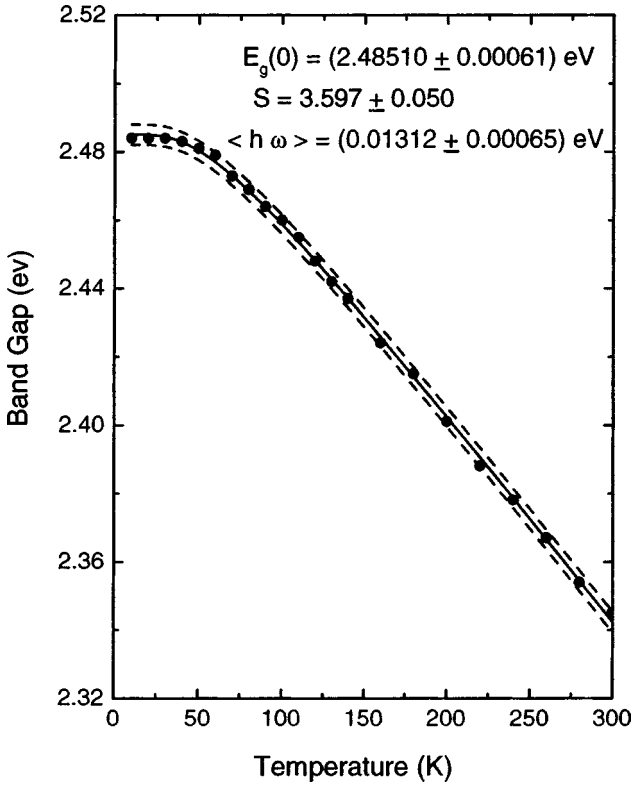

FIG. 2. Full circles are the experimentally determined values, with ABS measurements, for the band-gap energy of PbI_2 as a function of temperature. Curve shows the best fit to the experimental data obtained with the use of Eq. (4). Dashed points represent lower and upper error limits.

and 300 K. In the ABS measurements, light from a stabilized filament lamp was passed through the sample, the wavelength was analyzed in a 1 m grating spectrometer (McPherson model 2051) and detected with a photomultiplier (Hamamatsu model R 943-02), using a personal-computer-based single-photon-counting technique. Reference spectra were obtained by keeping the geometry of the setup fixed and removing the sample from the light path.

The absorption edge, i.e., where the signal of the transmitted light rose over and above the background level, could for all sample temperatures be determined with a small uncertainty (2 meV or less). The photon energy at the absorption edge is identified as the fundamental band-gap energy. In Figs. 1 and 2 the experimental results are shown versus the sample temperature.

Ellipsometric spectra of PbI_2 were recorded at room temperature with variable angle of incidence spectroscopic ellipsometry (J. A. Woollam, Inc. CO) in the photon energy range 1–5 eV in steps of 0.02 eV. Two angles of incidence were used: 60° and 70°. For line-shape analysis, high-resolution spectra were measured at three angles (50°, 60°, and 70°) with 0.005 eV steps in the photon energy range 2–3.5 eV.

The sample quality did not allow us to use a beam diameter larger than 1 mm. Further reduction of the beam size did not significantly change the data except that the noise level increased. Measurements were done on several spots on the sample and with different orientations but no significant variations were found. Generalized ellipsometry was used to determine all four elements of the reflection Jones matrix of the sample to resolve anisotropic effects. It was found that these effects, if present, were below what is detectable with the system used.

The measured Ψ and Δ spectra can be transformed directly to pseudodielectric function data $\langle\epsilon\rangle$. $\langle\epsilon\rangle$ would correspond to the real dielectric function $\langle\epsilon\rangle = \langle\epsilon_1 + i\epsilon_2\rangle$ of the substrate if it was ideal with no roughness or overlayers. However, ϵ_2 was found to be considerably above zero below the fundamental gap around 2.4 eV. The data were, therefore, interpreted in a model using a homogeneous substrate with a roughness layer. The latter was modeled using the Bruggeman effective medium approximation with 50% void and 50% substrate material as constituents. The Levenberg–Marquart algorithm was used to fit the model data to the experimental data. The thickness of the rough layer was a global fit parameter, whereas the dielectric function of the substrate was fitted on a wavelength by the wavelength basis. The thickness of the rough layer varied slightly between different spots on the sample but was of the order of 15 nm. In a particular spot, corresponding to the dielectric function data presented in this article, the thickness was 15 ± 3 nm, where the limits correspond to 90% confidence intervals.

III. THEORETICAL CALCULATIONS

In order to study the electronic structure of PbI_2, we have used the FPLMTO method.[10] The calculation were based on the local-density approximation with the Hedin–Lundqvist[11] parametrization for the exchange and

correlation potential. The spin-orbit coupling was included explicitly. Basis functions, electron densities, and potentials were calculated without any geometrical approximation.[9] These quantities were expanded in combinations of spherical harmonic functions (with a cutoff $\ell_{\max}=8$) inside nonoverlapping spheres surrounding the atomic sites (muffin-tin spheres) and in a Fourier series in the interstitial region. The muffin-tin spheres occupied approximately 60% of the unit cell. The radial basis functions within the muffin-tin spheres are linear combinations of radial wave functions and their energy derivatives, computed at energies appropriate to their site and principle as well as orbital atomic quantum numbers, whereas outside the muffin-tin spheres the basis functions are combinations of Neuman or Hankel functions.[12,13] In the calculations reported here, we made use of pseudocore $5d$ and $4d$ for Pb and I, respectively, and valence band $6s, 6p, 6d,$ and $5f$ basis functions for Pb and $5s, 5p, 5d$ and $4f$ basis functions for I with the corresponding two sets of energy parameters, one appropriate for the semicore $4d$ and $5d$ states, and the other appropriate for the valence states. The resulting basis formed a single, fully hybridizing basis set. This approach has previously proven to give a well converged basis.[10] For sampling the irreducible wedge of the Brillouin zone we used the special k-point method.[14] In order to speed up the convergence we have associated each calculated eigenvalue with a Gaussian broadening of width 10 mRy.

Calculation of the dielectric function

The $(q=0)$ dielectric function was calculated in the momentum representation, which requires the matrix elements of momentum $\mathbf{p}$ between occupied and unoccupied eigenstates. To be specific the imaginary part of the dielectric function, $\epsilon_2(\omega)\equiv \mathrm{Im}\ \epsilon(\mathbf{q}=0,\omega)$, was calculated from[15]

$$\epsilon_2^{ij}(\omega)=\frac{4\pi^2e^2}{\Omega m^2\omega^2}\sum_{\mathbf{k}nn'\sigma}\langle \mathbf{k}n\sigma|p_i|\mathbf{k}n'\sigma\rangle\langle \mathbf{k}n'\sigma|p_j|\mathbf{k}n\sigma\rangle \times f_{\mathbf{k}n}(1-f_{\mathbf{k}n'})\,\delta(e_{\mathbf{k}n'}-e_{\mathbf{k}n}-\hbar\omega). \quad (1)$$

In Eq. (1), e is the electron charge, m the electron mass, Ω is the crystal volume, and $f_{\mathbf{k}n}$ is the Fermi distribution function. Moreover, $|\mathbf{k}n\sigma\rangle$ is the crystal wave function corresponding to the nth eigenvalue with crystal momentum $\mathbf{k}$ and spin σ. With our spherical wave basis functions, the matrix elements of the momentum operator can be conveniently calculated in spherical coordinates and for this reason the momentum is written as $\mathbf{p}=\Sigma_\mu \mathbf{e}^*_\mu p_\mu$,[16] where μ is -1, 0, or 1, and $p_{-1}=1/\sqrt{2}(p_x-ip_y)$, $p_0=p_z$, and $p_1=-1/\sqrt{2}(p_x+ip_y)$.[17]

The evaluation of the matrix elements in Eq. (1) is done separately over the muffin-tin and the interstitial regions. The integration over the muffin-tin spheres is done in a way similar to the procedures used by Oppeneer[18] and Gasche.[15] However, their calculations utilized the atomic sphere approximation (ASA). A fully detailed description of the calculation of the matrix elements is presented elsewhere.[6]

The summation over the Brillouin zone in Eq. (1) is performed by using linear interpolation on a mesh of uniformly distributed points, i.e., the tetrahedron method. Matrix elements, eigenvalues, and eigenvectors are calculated in the irreducible part of the Brillouin zone. The correct symmetry for the dielectric constant was obtained by averaging the calculated dielectric function. Finally, the real part of the dielectric function, $\epsilon_1(\omega)$, is obtained from $\epsilon_2(\omega)$ using the Kramers–Kronig relation,

$$\epsilon_1(\omega)\equiv \mathrm{Re}[\,\epsilon(\mathbf{q}=0,\omega)\,] =1+\frac{1}{\pi}\int_0^\infty d\omega'\,\epsilon_2(\omega')\left(\frac{1}{\omega'-\omega}+\frac{1}{\omega'+\omega}\right). \quad (2)$$

TABLE I. Fit parameters of the temperature dependence from Eq. (4). PbI_2 from our data; other semiconductors are compiled from Ref. 8.

	$E_g(0)$ eV	S	$\hbar\,\omega$ meV
PbI_2	2.485	3.60	13.1
GaP	2.338	3.35	43.6
GaSb	1.521	3.00	26.7
Si	1.170	1.49	25.5

IV. RESULTS AND DISCUSSION

A. Temperature dependence of the band-gap energy

The relation usually employed for the temperature dependence of band-gap energy is that of Varshni:[7]

$$E_g(T)=E_g(0)-\frac{\alpha T^2}{T+\beta'}, \quad (3)$$

where $E_g(0)$ is the band-gap energy at $T=0$ K, and α and β are parameters characteristic of a given material, which are determined by fitting the right-hand equation to an experimental data set. Most semiconductors have a value of α around 10^{-4} eV/K. Here, we found for $E_g(0)=2.490$ eV, $\alpha=7.05\times10^{-4}$ eV/K, and $\beta=130$ K. The smooth curve shown in Fig. 1, was obtained by fitting Eq. (3) to the full squared data sets. Using another numerical least-square fitting procedure it is possible to extract the dependence of the band-gap energy more accurately from the O'Donnell and Chen relation:[8]

$$E_g(T)=E_g(0)-S\langle\hbar\omega\rangle\left[\coth\left(\frac{\langle\hbar\omega\rangle}{2k_\beta T}\right)-1\right], \quad (4)$$

where S is a dimensionless coupling constant, and $\langle\hbar\omega\rangle$ is an average phonon energy. For PbI_2 we obtain $E_g(0)=2.485$ eV, $S=3.60$, and $\langle\hbar\omega\rangle=13.1$ meV. It is worth to mention that this notation is adopted from the vibronic model of Huang and Rhys.[8,19]

The smooth curve shown in Fig. 2 is obtained by fitting Eq. (4) to the full circle data sets. Here, we notice a better fitting with Eq. (4) compared to Eq. (3).

In Table I we show the results obtained from Eq. (4) and compared them with other semiconductors. In Table II, we show the obtained band-gap energies for different temperatures utilizing PAS, TR, ABS measurements, and the two fitting procedures, O'Donnell and Chen (FDC) and Varshni (FV). In Table III, we present $\Delta E_g=E_g(T=0$ and 10 K$)-E_g(T=300$ K$)$ calculated from various sets of the ABS measurement as well as the FDC and FV fitting procedures.

TABLE II. Value of $E_g(T)$, obtained by PAS and ABS measurements and fitting procedures, FDC and FV representing by Eqs. (4) and (3), respectively.

Method	E_g (300 K) eV	E_g (10 K) eV	E_g (0 K) eV
PAS[a]	2.320±0.038	···	···
TR[b]	2.319±0.070	···	···
ABS[c]	2.345±0.037	2.484±0.042	···
FDC[d]	2.345±0.001	2.484±0.001	2.485±0.001
FV[e]	2.340±0.001	2.487±0.001	2.489±0.001
$[E_g(\text{ABS})-E_g(\text{PAS})]_{300\ \text{K}}$	25 meV		

[a]Photoacoustic spectroscopy.
[b]Transmission.
[c]Absorption.
[d]Fitting the O'Donnell and Chen equation to ABS curve.
[e]Fitting the Varshni equation.

For case (a) where $\Delta E_g = E_g(T=10\ \text{K}) - E_g(T=300\ \text{K})$, we have ABS=0.139, FDC=0.139, FV=0.147, and for case (b) where $\Delta E_g = E_g(T=0\ \text{K}) - E_g(T=300\ \text{K})$, we have FDC=0.140 and FV=0.149. We can see that the ΔE_g values of ABS and FDC are identical, but not those derived from FV.

B. Optical properties

Since the optical spectra are calculated from interband transitions, we find it of interest to first describe our calculated electronic structure. For this reason we show the calculated density of states (DOS) in Fig. 3. The major contributions to the total DOS come from the Pb *d* and Pb *s* states and the I *s* and I *p* states. The total DOS has many structures: (a) a peak around −14.0 eV arising from the I *s* states; (b) a narrow structure around −9.0 eV arising form the Pb *s* states; (c) a broad structure around −5.0 eV from the Pb *p* and I *p* states; and (d) a structure just after the band-gap arising from the antibonding Pb *p* and I *p* states. Our calculated band gap is around 1.5 eV, which is 0.85 eV lower than experiment. This type of error for band-gap energies is very usual in local density approximation (LDA) calculations.

The measured dielectric function is shown in Fig. 4. In Fig. 4(a), we show the imaginary part of dielectric function ϵ_2 and notice an onset of absorption around 2.4 eV. Below this gap there is some residual absorption, which may be real or due to model artifacts. Above the fundamental gap rather well-defined absorption bands are seen at 2.9 and 3.2 eV as well as a broad band between 4 and 4.5 eV. In Fig. 4(b) we show the real part of dielectric function ϵ_1. This exhibits a peak around 2.5 eV, a shoulder around 2.75 eV, a peak around 3.2 eV, and also a minimum at 4.5 eV. These features of ϵ_1 are also Kramers–Kronig consistent with ϵ_2.

TABLE III. Values of ΔE_g (0 K) and ΔE_g (10 K) for the ABS measurement and fitting procedures, FDC and FV.

Method	ΔE_g (10 K)[a] eV	ΔE_g (0 K)[b] eV
ABS	0.139	···
FDC	0.139	0.140
FV	0.147	0.149

[a]$\Delta E_g(10\ \text{K}) = E_g(10\ \text{K}) - E_g(300\ \text{K})$.
[b]$\Delta E_g(0\ \text{K}) = E_g(0\ \text{K}) - E_g(300\ \text{K})$.

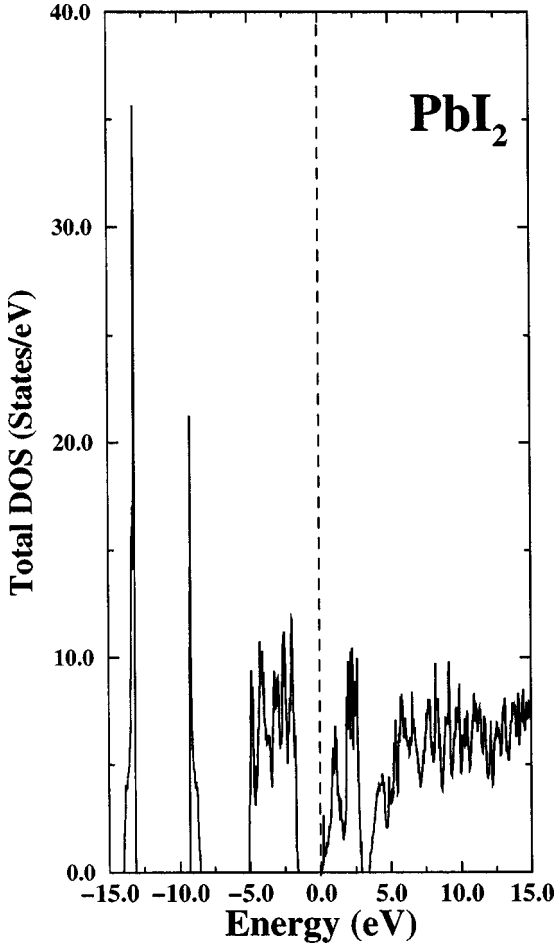

FIG. 3. Calculated total density of states (DOS) for PbI_2. Fermi energy has been set to the zero energy level and marked by a vertical dashed line.

In Fig. 5(a) we show the calculated imaginary part of dielectric functions $\epsilon_2^{\perp}$, $\epsilon_2^{\parallel}$, and ϵ_2^{tot}. Our calculated $\epsilon_2^{\perp}$ displays basically three main peaks; two at low energies and one at a higher energy. The two low-energy peaks are positioned around 3.0 and 4.0 eV and the high-energy peak is around 7.0 eV. However, for $\epsilon_2^{\parallel}$, the two peaks are found around 3.5 and 4.5 eV and the high-energy peak is at 7.0 eV. Our calculated spectra compare very well with the measured one. By comparing $\epsilon_2^{\perp}$ and $\epsilon_2^{\parallel}$, one can notice that the anisotropy of the dielectric function is very small. We have also investigated the origin of these peaks. The first two peaks, both in the parallel and the perpendicular directions, originate from Pb *s* to Pb *p* interband transitions while the peak at 7.0 eV originates from the Pb *p* to Pb *d* interband transition, since the LDA is well known for underestimation of the band gap and our band gap is 0.85 eV less compared to the experiment. If one uses a scissor operator to calculate the dielectric function using the experimental gap as done by several workers in the past, our whole spectra will shift by 0.85 eV towards higher energies. This will not improve the agreement with the experiment data. It means that one cannot just shift the band gap but one has to go beyond the LDA using a more sophisticated approach like the GW method,[20] where

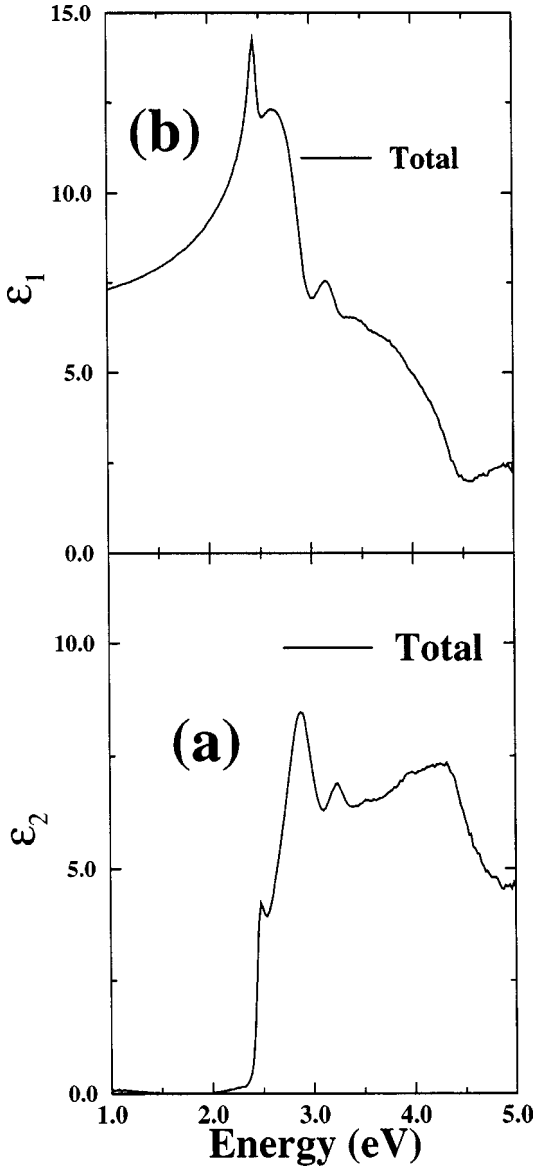

FIG. 4. Experimental total dielectric function as a function of photon energies (a) ϵ_2 and (b) ϵ_1.

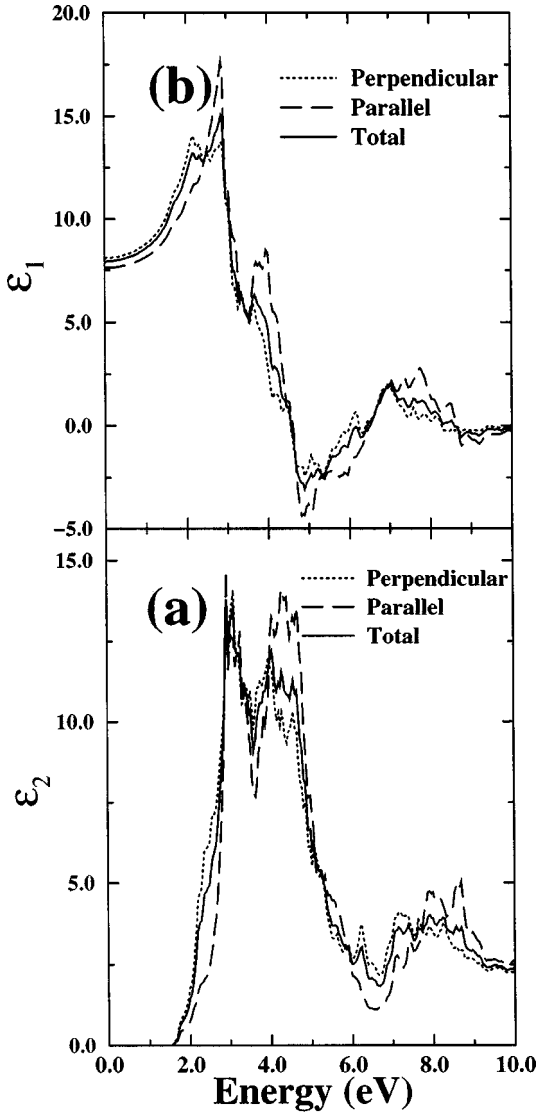

FIG. 5. Calculated dielectric function as a function of photon energy for different directions (a) ϵ_2 and (b) ϵ_1.

correlations are included. This approach does not just give a better band gap but also improves the electronic structure. In Fig. 5(b) we show the calculated real part of the dielectric function, $\epsilon_1^{\perp}$, $\epsilon_1^{\parallel}$, and $\epsilon_1^{\mathrm{tot}}$. The real part of the dielectric function is obtained from ϵ_2 by the Kramers–Kronig relation. Our calculated $\epsilon_1^{\perp}$ shows two sharp peaks and a broad peak. The first peak is situated around 3.0 eV, the second one is at 4.0 eV, and the broad peak is around 7.5 eV. $\epsilon_1^{\perp}$ becomes negative around 5.0 eV. The calculated $\epsilon_1^{\parallel}$ also has a very similar structure as $\epsilon_1^{\perp}$. In $\epsilon_1^{\parallel}$, there is an additional peak at around 2.0 eV, which is absent in $\epsilon_1^{\perp}$. At 1.0 eV, our calculated value of $\epsilon_1(0)$ is 7.5, which compares very well with the experimental value of 7.2.

V. CONCLUSIONS

We have studied the electronic and optical properties of PbI_2 using optical absorption, transmission, ellipsometry, and also theoretically using the FPLMTO method with spin-orbit coupling. Our calculations for the dielectric function compare well with experiments. Our calculations show that there is a very small anisotropy in the optical properties of PbI_2. This is in contrast to what our previous calculations on HgI_2 (Ref. 21) have shown. Our calculated and experimental values of $\epsilon_1(0)$ are in very good agreement. The measured band gap determined from different methods are consistent with each other.

ACKNOWLEDGMENTS

Three of the authors (A.F.S., J.S.A., and N.V.) acknowledge support from the Brazilian National Research Council, CNPq. Two of the authors (R.A. and B. J.) acknowledge the Swedish Research Council (VR). One of the authors (E.V.) is very grateful for the support from the Danish Natural Science Research Council, the Carlsberg Foundation, Director Ib Henriksens Foundation, and NOVO Nordic Foundation.

[1] K. S. Shah, F. Olschner, L. P. Moy, P. Bennett, M. Misra, J. Zhang, M. R. Squillante, and J. C. Lund, Nucl. Instrum. Methods Phys. Res. A **380**, 266 (1996).
[2] T. Shogi, K. Ohba, T. Suchiro, and Y. Hiratate, IEEE Trans. Nucl. Sci. **41**, 694 (1994); **42**, 659 (1995).
[3] A. Burger, S. H. Morgan, E. Silberman, D. Nason, and A. Y. Cheng, Nucl. Instrum. Methods Phys. Res. A **322**, 427 (1992).
[4] A. Ferreira da Silva, N. Veissid, C. Y. An, I. Pepe, N. Barros de Oliveira, and A. V. Batista da Silva, Appl. Phys. Lett. **69**, 1930 (1996).
[5] T. S. Silva, A. S. Alves, I. Pepe, H. Tsuzuki, O. Nakamura, M. M. F. Aguiar Neto, A. Ferreira da Silva, N. Veissid, and C. Y. An, J. Appl. Phys. **83**, 6193 (1998).
[6] R. Ahuja, S. Auluck, J. M. Wills, M. Alouani, B. Johansson, and O. Eriksson, Phys. Rev. B **55**, 4999 (1997).
[7] Y. P. Varshni, Physica (Amsterdam) **34**, 149 (1967).
[8] K. P. O'Donnell and X. Chen, Appl. Phys. Lett. **58**, 2924 (1991).
[9] R. Ahuja, A. Ferreira da Silva, C. Persson, J. M. Osorio-Guillen, I. Pepe, K. Järrendahl, O. P. A. Lindqvist, N. V. Edwards, Q. Wahab, and B. Johansson, J. Appl. Phys. **91**, 2099 (2002).
[10] J. M. Wills (unpublished); J. M. Wills and B. R. Cooper, Phys. Rev. B **36**, 389 (1987); D. L. Price and B. R. Cooper, *ibid.* **39**, 4945 (1989).
[11] L. Hedin and B. I. Lundqvist, J. Phys. C **4**, 2064 (1971).
[12] O. K. Andersen, Phys. Rev. B **12**, 3060 (1975).
[13] H. L. Skriver, *The LMTO Method* (Springer, Berlin, 1984).
[14] D. J. Chadi and M. L. Cohen, Phys. Rev. B **8**, 5747 (1973); S. Froyen, *ibid.* **39**, 3168 (1989).
[15] A good description of the calculation of dielectric constants and related properties are found in the thesis by T. Gashe, Uppsala University (1993).
[16] A. R. Edmonds, *Angular Momentum in Quantum Mechanics* (Princeton University Press, Princeton, NJ, 1974), p. 82.
[17] In practice, we calculate matrix elements of the symmetrized momentum operator $\langle i|\vec{\mathbf{p}}_\mu big|j\rangle \equiv (\langle i|p_\mu j\rangle + (-1)^\mu \langle p_{-mu} i|j\rangle)/2$.
[18] P. Oppeneer, T. Maurer, J. Sticht, and J. Kübler, Phys. Rev. B **45**, 10924 (1992).
[19] K. Huang and A. Rhys, Proc. R. Soc. London, Ser. A **204**, 406 (1950).
[20] R. Del Sole, L. Reining, and R. W. Godby, Phys. Rev. B **49**, 8024 (1994).
[21] R. Ahuja, O. Eriksson, B. Johansson, S. Auluck, and J. M. Wills, Phys. Rev. B **54**, 10419 (1996).